SCIENCE CHINA
Information Sciences

• RESEARCH PAPER •

April 2021, Vol. 64 140404:1–140404:7
https://doi.org/10.1007/s11432-020-3101-1

Special Focus on Two-Dimensional Materials and Device Applications

Bi_2O_2Se/BP van der Waals heterojunction for high performance broadband photodetector

Xing LIU, Wenhui WANG, Fang YANG, Shaopeng FENG, Zhenliang HU,
Junpeng LU* & Zhenhua NI*

School of Physics, Southeast University, Nanjing 211189*, China*

Received 18 September 2020/Revised 16 October 2020/Accepted 26 October 2020/Published online 2 March 2021

Abstract Broadband photodetector has wide applications in the field of remote sensing, health monitoring and medical imaging. Two-dimensional (2D) materials with narrow bandgaps have shown enormous potential in broadband photodetection. However, the device performance is often restricted by the high dark currents. Herein, we demonstrate a high performance broadband photodetector by constructing Bi_2O_2Se/BP van der Waals heterojunction. The device exhibits a p-n diode behavior with a current rectification ratio of ∼20. Benifited from the low dark current of the heterojunction and the effective carrier separation, the device achieves the responsivity (R) of ∼ 500 A/W, ∼ 4.3 A/W and ∼ 2.3 A/W at 700 nm, 1310 nm and 1550 nm, respectively. The specific detectivity (D*) is up to $\sim 2.8 \times 10^{11}$ Jones (700 nm), $\sim 2.4 \times 10^9$ Jones (1310 nm) and $\sim 1.3 \times 10^9$ Jones (1550 nm). Moreover, the response time is ∼ 9 ms, which is more than 20 times faster than that of individual BP (∼ 190 ms) and Bi_2O_2Se (∼ 180 ms) devices.

Keywords Bi_2O_2Se/BP, van der Waals heterojunction, broadband photodetector, low dark current, narrow bandgap

Citation Liu X, Wang W H, Yang F, et al. Bi_2O_2Se/BP van der Waals heterojunction for high performance broadband photodetector. Sci China Inf Sci, 2021, 64(4): 140404, https://doi.org/10.1007/s11432-020-3101-1

1 Introduction

Photodetectors based on two dimensional (2D) layered semiconductor materials have been widely studied owing to their ultra-thin characteristics, strong light absorption and tunable optoelectronics properties [1,2]. A variety of narrow bandgap 2D semiconductors have been explored for broadband photodetection, such as black phosphorus (BP) [3,4], black arsenic phosphorus (AsP) [5,6] and bismuth oxyselenide (Bi_2O_2Se) [7,8]. High responsivity and detectivity have been achieved in these broadband 2D photodetectors. However, these 2D photodetectors with high responsivity are often operated in photoconductive mode, which suffer from high dark current and slow response speed [9,10]. Generally, a good photodetectors needs to have high sensitivity, fast response speed, broadband response and high detectivity, which are rare to meet simultaneously in individual 2D material. Van der Waals (vdW) heterojunction provides an alternative platform to satisfy the requirements above simultaneously [11–13]. The built-in electrical field (E_{in}) generated at the junction region can be utilized to suppress dark current and separate the photogenerated electron-hole pairs for fast photoelectric conversion [12–14]. Therefore, constructing vdW heterojunction will help solve the problems of high dark current in narrow bandgap 2D material based photodetector and achieve high performance broadband photodetection.

Herein, we design a vdW heterojunction photodetector based on Bi_2O_2Se and BP thin flakes. The Bi_2O_2Se/BP heterojunction exhibits a diode behavior with a current rectification ratio of ∼ 20. Utilizing the dual absorption and the effective carrier separation, the device demonstrates high responsivity (R) of ∼500 A/W, ∼ 9.5 A/W, ∼ 4.3 A/W and ∼ 2.3 A/W at 700 nm, 850 nm, 1310 nm, and 1550 nm, respectively. Benefit from the low dark current of the heterojunction, the specific detectivity (D*) under 700 nm illumination reaches $\sim 2.8 \times 10^{11}$ Jones, which is two orders of magnitude higher than that of BP

* Corresponding author (email: phyljp@seu.edu.cn, zhni@seu.edu.cn)

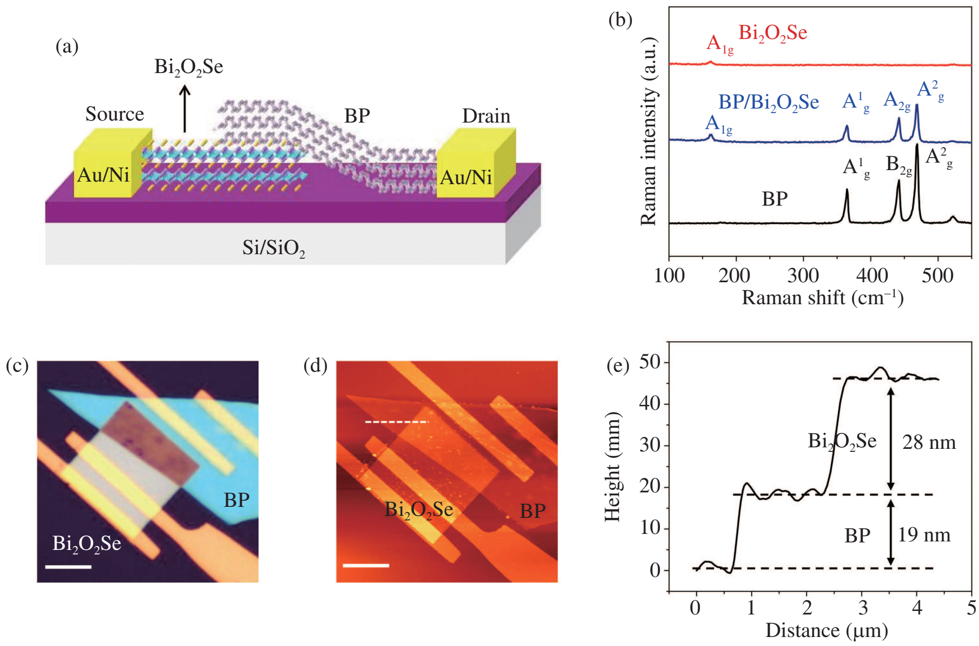

Figure 1 (Color online) Structural characterizations of Bi_2O_2Se/BP vdW heterojunction. (a) Schematic of the Bi_2O_2Se/BP vdW heterojunction photodetector. (b) Raman spectra of BP, Bi_2O_2Se, and Bi_2O_2Se/BP heterojunction regions. (c) and (d) Optical and AFM images of the device. The scale bar is 6 μm. (e) Height profile of BP and Bi_2O_2Se flakes corresponding to the white line marked in (d).

($\sim 3.0 \times 10^9$ Jones) and Bi_2O_2Se ($\sim 3.8 \times 10^9$ Jones) devices. In addition, the fast response speed of ~ 9 ms is achieved, more than 20 times faster than the photodetectors built on BP (~ 190 ms) and Bi_2O_2Se (~ 180 ms). This heterojunction photodiode with high performance and broadband photodetection provides an important platform for the application of photodetector.

2 Results and discussion

(1) Architecture of Bi_2O_2Se/BP vdW heterojunction. Figure 1(a) shows a schematic view of the Bi_2O_2Se /BP vdW heterojunction device, constructing by stacking BP thin flake on top of 2D Bi_2O_2Se thin flake. 2D Bi_2O_2Se flake was synthesized on a mica surface by chemical vapor deposition (CVD) methods and transferred onto a 300 nm SiO_2/Si substrate by using the PMMA-mediated method (see Figure S1). BP thin flake was then transferred onto the Bi_2O_2Se flake using polydimethylsiloxane (PDMS) as the supporting substrate. Thereafter, the 5 nm/50 nm Ni/Au electrodes were patterned using the standard e-beam lithography and deposited using a thermal evaporator. The optical and atomic force microscope (AFM) images of the heterojunction are shown in Figures 1(c) and (d). From the AFM profile (Figure 1(e)), the thicknesses of the Bi_2O_2Se and BP layers are ~ 28 nm and ~ 19 nm, respectively. The Raman spectra are collected and shown in Figure 1(b). Three characteristic peaks at ~ 364, ~ 440, and ~ 468 cm^{-1} correspond to A^1_g, B^2_g, and A_{2g} modes of BP thin flake [15], respectively. As for Bi_2O_2Se, the characteristic peak, A_{1g}, at ~ 160 cm^{-1}can be observed [16]. In addition, the Raman characteristic peaks of both BP and Bi_2O_2Se can be clearly observed in the Bi_2O_2Se/BP heterojunction region and no shift was observed compared to the spectra of the individual flakes, signifying good crystal quality of each component in the heterojunction.

(2) Electrical characterizations of Bi_2O_2Se/BP vdW heterojunction. Transfer characteristics of the Bi_2O_2Se and BP field effect transistors (FET) are shown in Figure 2(a). All the electrical characteristics of the devices were measured under room temperature atmosphere by using a Keithley 2612 analyzer. BP shows a typical p-type behavior [17] and Bi_2O_2Se shows a typical n-type behavior [7]. The hole mobility in BP FET is calculated to be ~ 180 cm^2/Vs and the electron mobility in Bi_2O_2Se FET is calculated to be ~ 123 cm^2/Vs. Output characteristics are also measured and shown in Figure S2. Both devices exhibit almost symmetric I_{ds}-V_{ds} curves, indicating good contact with the Ni/Au electrodes. With p-type characteristics in BP and n-type characteristics in Bi_2O_2Se, the vertically stacked Bi_2O_2Se/BP

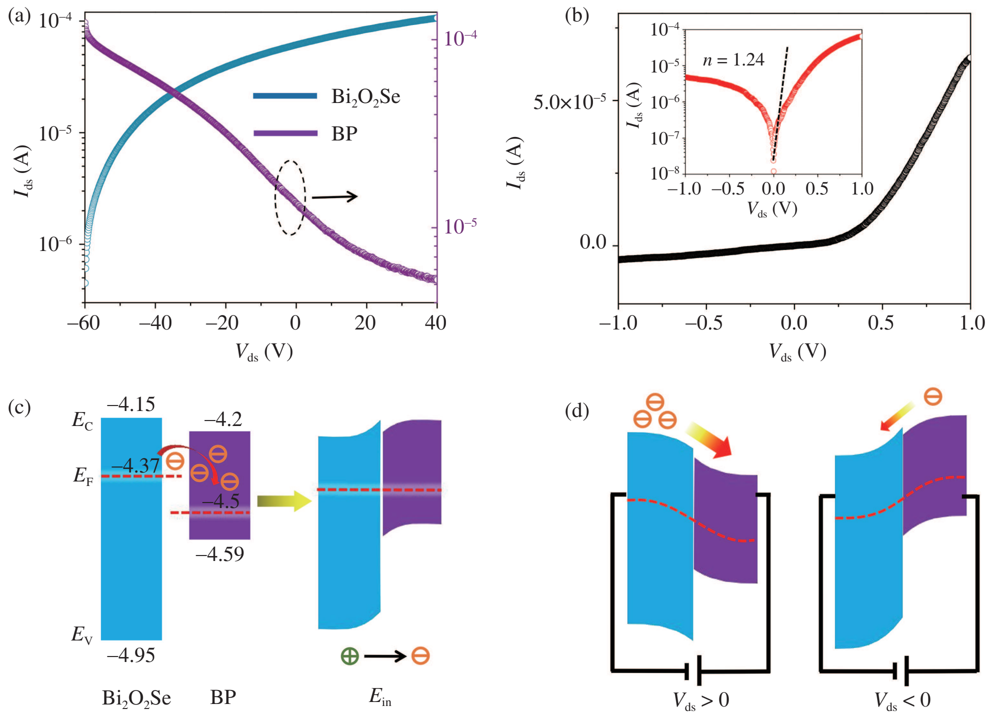

Figure 2 (Color online) Electrical characterizations of the Bi_2O_2Se/BP vdW heterojunction. (a) The transfer characteristics of the Bi_2O_2Se FET and BP FET. (b) I_{ds}-V_{ds} characteristic of the Bi_2O_2Se/BP vdW heterojunction. The inset shows the curve plotted on logarithmic scale. (c) Energy band diagram of the BP/Bi_2O_2Se vdW heterojunction at equilibrium before and after contact. (d) Energy band diagrams of the Bi_2O_2Se/BP vdW heterojunction device under different bias voltage V_{ds}.

heterojunction forms a natural p-n junction [18]. Figure 2(b) shows the I_{ds}-V_{ds} curve of the Bi_2O_2Se/BP p-n junction, where drain bias is applied to the BP. The $I_{ds} - V_{ds}$ curve reveals a typical p-n diode-like current rectification behavior and possesses a rectification ratio of $\sim$ 20. In addition, the fitted ideality factor of the diode is ∼1.24 [19], indicating a high quality heterojunction interface.

According to the previously reported measurements results and first-principles density of states in the literature, the conduction band minimum (E_C), valence band maximum (E_V) and Fermi level (E_F) of the BP (Bi_2O_2Se) locate at $\sim$ −4.2 eV (−4.15 eV), −4.59 eV (−4.95 eV) and −4.5 eV (−4.37 eV), respectively [20–24]. Figure 2(c) describes the predicted energy band diagram of Bi_2O_2Se/BP heterojunction at equilibrium before and after contact. The large work function difference leads to the accumulation of holes in Bi_2O_2Se and electrons in BP, and forms a natural p-n junction in the device. In order to understand the mechanism of the diode-like rectification observed in the Bi_2O_2Se/BP heterojunction, we drew the energy band diagrams under both forward and reverse bias conditions (Figure 2(d)). Under forward bias, the built-in electric field of the heterojunction is compensated by the external electric field, which is beneficial for electrons (majority carriers) transfer from Bi_2O_2Se to BP and resulting in an increase in the current. On the other hand, the reverse bias enhances the built-in electric field. It widens the depletion region and increases the potential barrier, which decreases the current and generates the current-rectifying characteristics of the junction [25].

(3) Optoelectronic characteristics of the Bi_2O_2Se/BP vdW heterojunction. Figure 3(a) shows the I_{ds}-V_{ds} curves of the device under dark and 700 nm focused laser illumination with different incident powers. A Chameleon with Compact OPO (Coherent Inc.) was used as light source. With increasing light power, the channel current gradually increases under the negative bias. Figure 3(b) presents the magnified I_{ds}-V_{ds} curves. The negative short circuit current (I_{sc}) and positive open circuit voltage (V_{oc}) indicate the photovoltaic effect of the device [19]. The photocurrent, I_{ph} (defined as $I_{ph} = I_{light} - I_{dark}$), is extracted from the I_{ds}-V_{ds} curves and plotted in Figure 3(c). Larger I_{ph} can be obtained under negative bias, demonstrating the higher photoresponse at reverse bias regime. Scanning photocurrent mapping is used to distinguish the photocurrent domain. The photocurrent mapping were conducted using a Witec confocal Raman system with Ar ion laser (532 nm) excitation. As shown in Figure 3(d), a strong photocurrent is observed in the junction area and no obvious photocurrent is observed at bare Bi_2O_2Se

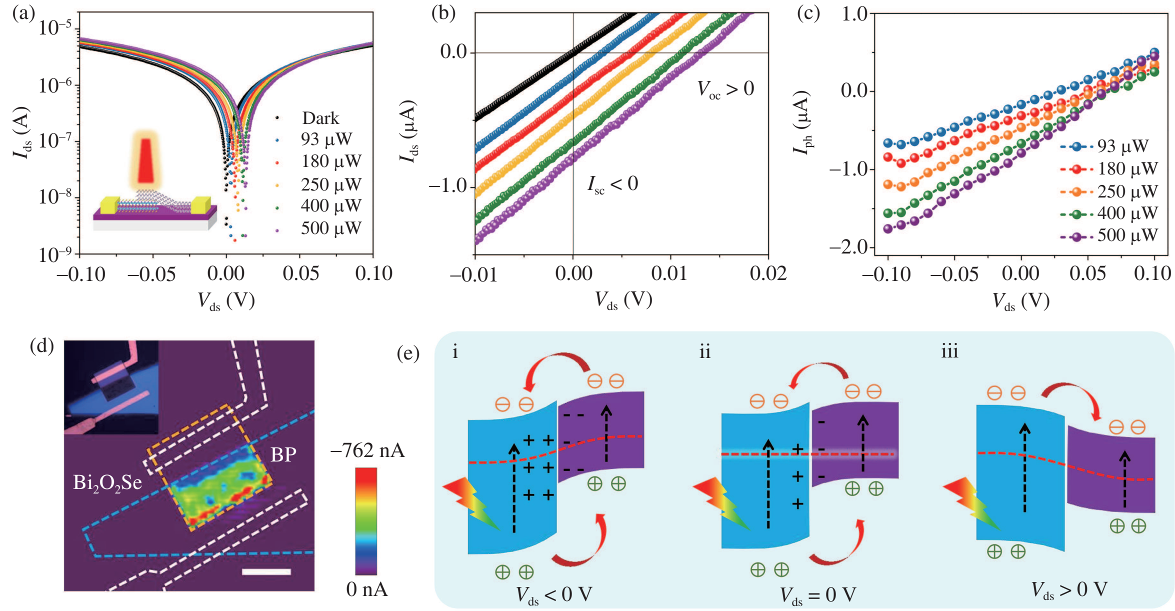

Figure 3 (Color online) Photoresponse of the Bi_2O_2Se/BP vdW heterojunction. (a) Power depended I_{ds}-V_{ds} curves under 700 nm laser illumination. The inset is the schematic diagram of the Bi_2O_2Se/BP vdW heterojunction based photovoltaic device. (b) The enlarged view of the I_{ds}-V_{ds} curves in (a). (c) The photocurrent extracted from (b). (d) Scanning photocurrent mapping of the device under 532 nm laser illumination at V_{ds} = 0 V. The scale bar is 10 μm. (e) Energy band diagram of the Bi_2O_2Se/BP vdW heterojunction under 700 nm laser illumination at reverse (i), zero (ii), forward (iii) bias.

and BP regions. It unambiguously certifies the photocurrent indeed originates from the Bi_2O_2Se/BP heterojunction [10]. To explain the photovoltaic phenomenon, an energy band schematic diagram of the device under light illumination is shown in Figure 3(e). Under illumination, electron-hole pairs are generated in the both Bi_2O_2Se and BP. At the junction region, the electrons are driven to Bi_2O_2Se while the holes are driven to BP by the built-in electric field, thus resulting in positive V_{oc} and negative I_{sc} (Figure 3(b)). When a reverse bias is applied to the device (Figure 3(e-i)), the width of the depletion region and potential barrier increases. It enhances the separation of the carriers and increases the photocurrent. On the contrary, the forward bias compensates the built-in electric field (Figure 3(e-iii)), which narrows the depletion region and decreases the photocurrent [2].

Figure 4(a) shows the power depended responsivity of BP, Bi_2O_2Se and Bi_2O_2Se/BP heterojunction under visible light (700 nm) irradiation. All measurements are performed under −1 V bias voltage. The highest R (defined as $R = \frac{I_{\rm ph}}{P}$) of the heterojunction is ∼ 500 A/W, which is higher than that of BP (∼ 55 A/W), Bi_2O_2Se (∼ 225 A/W) device. D^* used to demonstrate the ability of the device to detect minimum illumination signal. By using $D* = \frac{\sqrt{S}R}{\sqrt{2eI_{\rm dark}}}$ (S is the area of the device), we have calculated the specific detectivity of D^*, which is also shown in Figure 4(b). Because of the low dark current of the heterojunction (Figure S2), the D^* of the Bi_2O_2Se/BP device is up to ∼ 2.8 × 10^{11} Jones, which is nearly two orders of magnitude higher than that of individual BP (∼ 3.0 × 10^9 Jones) and Bi_2O_2Se devices (∼ 3.8 × 10^9 Jones). Figure 4(c) shows the photo-switching characteristics. The response times of Bi_2O_2Se/BP, BP, Bi_2O_2Se are extracted from the falling edges to be ∼ 9 ms, ∼ 190 ms, and ∼ 180 ms, respectively (Figure 4(d)). The fast response speed of heterojunction is owning to the fast carrier separation at the interface, by which the trapping effect is reduced [14, 26]. However, carriers still suffer from the effects of traps arising from defects in the flakes during the lateral transport. Therefore, the response speed of heterojunction could be further improved by employing higher quality crystals or shortening the lateral channel length. The photoresponse of Bi_2O_2Se/BP heterojunction to near infrared light (850, 1310 and 1550 nm) are shown in Figures S3 and S4. Interestingly, the device also shows a fast response time (∼20 ms) under 1550 nm infrared light (Figure S5). The R and D^* are extracted and shown in Figure 4(e). Because of the absorption of both BP and Bi_2O_2Se to infrared light, R reaches ∼ 9.5 A/W, ∼ 4.3 A/W and ∼ 2.3 A/W at 850 nm, 1330 nm and 1550 nm, respectively. This is at a superior level among the BP or Bi_2O_2Se based photovoltaic photodetectors, as summarized in Figure 4(f) [27–38]. Whilst D^* is calculated to be ∼ 5.3 × 10^9 Jones, ∼ 2.4 × 10^9 Jones and ∼ 1.3

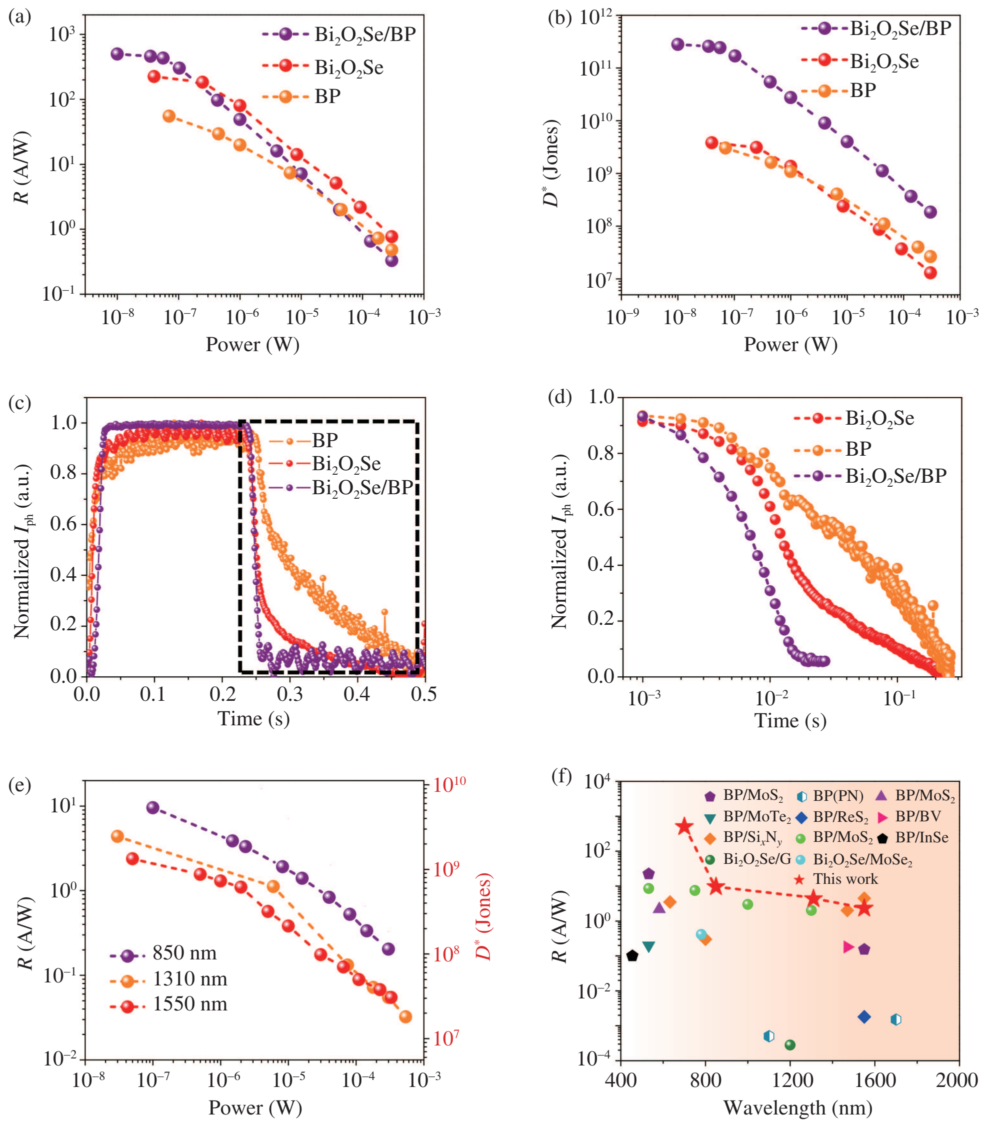

Figure 4 (Color online) High performance of the Bi_2O_2Se/BP vdW heterojunction photodetector. (a) and (b) Power depended R and D^* of Bi_2O_2Se, BP, and Bi_2O_2Se/BP heterojunction under 700 nm illumination at $V_{ds} = -1$ V. (c) Photoswitching response under 700 nm laser illumination at $V_{ds} = -1$ V. (d) The extracted response time from the falling edge in (c). (e) Power depended R and D^* of the Bi_2O_2Se/BP vdW heterojunction photodetector under three near-infrared waveband light (850 nm, 1310 nm and 1550 nm) at $V_{ds} = -1$ V. (f) Comparison of the R of Bi_2O_2Se/BP vdW heterojunction with other photovoltaic photodetectors based on BP and Bi_2O_2Se vdW heterojunction.

$\times\ 10^9$ Jones, respectively. The degradation of photoresponse at near infrared can be attributed to the decreasing absorption of BP and Bi_2O_2Se at the near infrared band [20, 39].

3 Conclusion

In summary, a broadband photodetector with high performance has been demonstrated based on Bi_2O_2Se/BP vdW heterojunction. It possesses responsivity of $\sim$ 500 A/W, $\sim$ 9.5 A/W, $\sim$ 4.3 A/W, and $\sim$ 2.3 A/W at spectral regions of 700 nm, 850 nm, 1310 nm and 1550 nm. Benefiting from the rectification effect and the low dark current of the p-n heterojunction, the detectivity of the device can reach up to $\sim 2.8 \times 10^{11}$ Jones (700 nm), $\sim 5.3 \times 10^9$ Jones (850 nm), $\sim 2.4 \times 10^9$ Jones (1310 nm) and $\sim 1.3 \times 10^9$ Jones (1550 nm). In addition, the fast separation of carriers at the Bi_2O_2Se/BP heterojunction enables a faster response time ($\sim$ 9 ms), which is more than 20 times faster than individual BP ($\sim$ 190 ms) and Bi_2O_2Se ($\sim$180 ms) photodetectors.

Acknowledgements This work was supported by National Key Research and Development Program of China (Grant Nos. 2017YFA0205700, 2019YFA0308000), National Natural Science Foundation of China (Grant Nos. 61774034, 91963130, 11704068, 61705106), Jiangsu Natural Science Foundation (Grant No. BK20170694), and the Fundamental Research Funds for the Central Universities.

Supporting information Figures S1–S5. The supporting information is available online at info.scichina.com and link.springer.com. The supporting materials are published as submitted, without typesetting or editing. The responsibility for scientific accuracy and content remains entirely with the authors.

References

1 Koppens F H L, Mueller T, Avouris P, et al. Photodetectors based on graphene, other two-dimensional materials and hybrid systems. Nat Nanotech, 2014, 9: 780–793

2 Buscema M, Island J O, Groenendijk D J, et al. Photocurrent generation with two-dimensional van der Waals semiconductors. Chem Soc Rev, 2015, 44: 3691–3718

3 Suess R J, Leong E, Garrett J L, et al. Mid-infrared time-resolved photoconduction in black phosphorus. 2D Mater, 2016, 3: 041006

4 Buscema M, Groenendijk D J, Blanter S I, et al. Fast and broadband photoresponse of few-layer black phosphorus field-effect transistors. Nano Lett, 2014, 14: 3347–3352

5 Liu B, Köpf M, Abbas A N, et al. Black arsenic-phosphorus: layered anisotropic infrared semiconductors with highly tunable compositions and properties. Adv Mater, 2015, 27: 4423–4429

6 Yuan S, Shen C, Deng B, et al. Air-stable room-temperature mid-infrared photodetectors based on hBN/black arsenic phosphorus/hBN heterostructures. Nano Lett, 2018, 18: 3172–3179

7 Fu Q, Zhu C, Zhao X, et al. Ultrasensitive 2D Bi_2O_2Se phototransistors on silicon substrates. Adv Mater, 2019, 31: 1804945

8 Li J, Wang Z, Wen Y, et al. High-performance near-infrared photodetector based on ultrathin Bi_2O_2Se nanosheets. Adv Funct Mater, 2018, 28: 1706437

9 Wang J, Fang H, Wang X, et al. Recent progress on localized field enhanced two-dimensional material photodetectors from ultraviolet-visible to infrared. Small, 2017, 13: 1700894

10 Wu F, Li Q, Wang P, et al. High efficiency and fast van der Waals hetero-photodiodes with a unilateral depletion region. Nat Commun, 2019, 10: 4663

11 Jin C, Ma E Y, Karni O, et al. Ultrafast dynamics in van der Waals heterostructures. Nat Nanotech, 2018, 13: 994–1003

12 Lee C H, Lee G H, van der Zande A M, et al. Atomically thin p-n junctions with van der Waals heterointerfaces. Nat Nanotech, 2014, 9: 676–681

13 Fang H, Battaglia C, Carraro C, et al. Strong interlayer coupling in van der Waals heterostructures built from single-layer chalcogenides. Proc Natl Acad Sci USA, 2014, 111: 6198–6202

14 Massicotte M, Schmidt P, Vialla F, et al. Picosecond photoresponse in van der Waals heterostructures. Nat Nanotech, 2016, 11: 42–46

15 Wang C, He Q, Halim U, et al. Monolayer atomic crystal molecular superlattices. Nature, 2018, 555: 231–236

16 Yang F, Wang R, Zhao W, et al. Thermal transport and energy dissipation in two-dimensional Bi_2O_2Se. Appl Phys Lett, 2019, 115: 193103

17 Doganov R A, O'Farrell E C T, Koenig S P, et al. Transport properties of pristine few-layer black phosphorus by van der Waals passivation in an inert atmosphere. Nat Commun, 2015, 6: 6647

18 Frisenda R, Molina-Mendoza A J, Mueller T, et al. Atomically thin p-n junctions based on two-dimensional materials. Chem Soc Rev, 2018, 47: 3339–3358

19 Liu H, Zhu X, Sun X, et al. Self-powered broad-band photodetectors based on vertically stacked WSe_2/Bi_2Te_3 p-n heterojunctions. ACS Nano, 2019, 13: 13573–13580

20 Luo P, Zhuge F, Wang F, et al. PbSe quantum dots sensitized high-mobility Bi_2O_2Se nanosheets for high-performance and broadband photodetection beyond 2 μm. ACS Nano, 2019, 13: 9028–9037

21 Shim J, Oh S, Kang D H, et al. Phosphorene/rhenium disulfide heterojunction-based negative differential resistance device for multi-valued logic. Nat Commun, 2016, 7: 13413

22 Cai Y, Zhang G, Zhang Y W. Layer-dependent band alignment and work function of few-layer phosphorene. Sci Rep, 2015, 4: 6677

23 Wu J, Yuan H, Meng M, et al. High electron mobility and quantum oscillations in non-encapsulated ultrathin semiconducting Bi_2O_2Se. Nat Nanotech, 2017, 12: 530–534

24 Srivastava P K, Hassan Y, Gebredingle Y, et al. Van der Waals broken-gap p-n heterojunction tunnel diode based on black phosphorus and rhenium disulfide. ACS Appl Mater Interfaces, 2019, 11: 8266–8275

25 Liu H, Li D, Ma C, et al. Van der Waals epitaxial growth of vertically stacked Sb_2Te_3/MoS_2 p-n heterojunctions for high performance optoelectronics. Nano Energy, 2019, 59: 66–74

26 Yu Y, Sun Y, Hu Z, et al. Fast photoelectric conversion in the near-infrared enabled by plasmon-induced hot-electron transfer. Adv Mater, 2019, 31: 1903829

27 Zhao S, Wu J, Jin K, et al. Highly polarized and fast photoresponse of black phosphorus-InSe vertical p-n heterojunctions. Adv Funct Mater, 2018, 28: 1802011

28 Xie Y, Wu E, Zhang J, et al. Gate-tunable photodetection/voltaic device based on $BP/MoTe_2$ heterostructure. ACS Appl Mater Interfaces, 2019, 11: 14215–14221

29 Zhu W, Wei X, Yan F, et al. Broadband polarized photodetector based on $p\text{-}BP/n\text{-}ReS_2$ heterojunction. J Semicon, 2019, 40: 092001

30 Zheng S, Wu E, Feng Z, et al. Acoustically enhanced photodetection by a black phosphorus-MoS_2 van der Waals heterojunction p-n diode. Nanoscale, 2018, 10: 10148–10153

31 Jiang X, Zhang M, Liu L, et al. Multifunctional black phosphorus/MoS_2 van der Waals heterojunction. Nanophotonics, 2020, 9: 2487–2493

32 Hong T, Chamlagain B, Wang T, et al. Anisotropic photocurrent response at black phosphorus-MoS_2 p-n heterojunctions. Nanoscale, 2015, 7: 18537–18541

33 Ye L, Li H, Chen Z, et al. Near-infrared photodetector based on MoS_2/black phosphorus heterojunction. ACS Photonics, 2016, 3: 692–699

34 Xu Y, Liu C, Guo C, et al. High performance near infrared photodetector based on in-plane black phosphorus p-n homojunction. Nano Energy, 2020, 70: 104518

35 Yu X, Zhang S, Zeng H, et al. Lateral black phosphorene P-N junctions formed via chemical doping for high performance near-infrared photodetector. Nano Energy, 2016, 25: 34–41

36 Yang T, Li X, Wang L, et al. Broadband photodetection of 2D Bi_2O_2Se-$MoSe_2$ heterostructure. J Mater Sci, 2019, 54: 14742–14751

37 Tan C, Xu S, Tan Z, et al. Exploitation of Bi_2O_2Se/graphene van der Waals heterojunction for creating efficient photodetectors and short-channel field-effect transistors. InfoMat, 2019, 1: 390–395

38 Yuan H, Liu X, Afshinmanesh F, et al. Polarization-sensitive broadband photodetector using a black phosphorus vertical p-n junction. Nat Nanotech, 2015, 10: 707–713

39 Guo Z, Zhang H, Lu S, et al. From black phosphorus to phosphorene: basic solvent exfoliation, evolution of raman scattering, and applications to ultrafast photonics. Adv Funct Mater, 2015, 25: 6996–7002